Hindawi
International Journal of Photoenergy
Volume 2018, Article ID 9704346, 9 pages
https://doi.org/10.1155/2018/9704346

Research Article

A New Multilevel Inverter Topology for Grid-Connected Photovoltaic Systems

Muhammad Bilal Satti,[1] **Ammar Hasan**,[1] **and Mian Ilyas Ahmad**[2]

[1]*School of Electrical Engineering and Computer Science (SEECS), National University of Science and Technology, Islamabad, Pakistan*
[2]*Research Center for Modeling and Simulation (RCMS), National University of Sciences and Technology (NUST), Islamabad, Pakistan*

Correspondence should be addressed to Muhammad Bilal Satti; msatti.msee15seecs@seecs.edu.pk

Received 19 March 2018; Revised 9 July 2018; Accepted 15 July 2018; Published 9 September 2018

Academic Editor: Pierluigi Guerriero

The demand for clean and sustainable energy has spurred research in all forms of renewable energy sources, including solar energy from photovoltaic systems. Grid-connected photovoltaic systems (GCPS) provide an effective solution to integrate solar energy into the existing grid. A key component of the GCPS is the inverter. The inverter can have a significant impact on the overall performance of the GCPS, including maximum power point (MPP) tracking, total harmonic distortion (THD), and efficiency. Multilevel inverters are one of the most promising classes of converters that offer a low THD. In this paper, we propose a new multilevel inverter topology with the motivation to improve all the three aforementioned aspects of performance. The proposed topology is controlled through direct model predictive control (DMPC), which is state of the art in control techniques. We compare the performance of the proposed topology with the topologies reported in literature. The proposed topology offers one of the best efficiency, MPP tracking, and voltage THD.

1. Introduction

At present, one of the key research areas in renewable energy are grid-connected photovoltaic systems (GCPS). The cost reduction of photovoltaic (PV) panels, environmental benefits, increased demand of energy, integration with existing grid, and advances in power electronics are some of the reasons for the focus on GCPS [1]. In a GCPS, the key performance criteria are conversion efficiency, maximum power point (MPP) tracking, and total harmonic distortion (THD) of the power injected into the grid. All these performance criteria are highly dependent on the choice of the inverter topology and the control technique utilized for the inverter.

In the literature, several topologies of inverters have been reported that can be used in a GCPS [2]. Multilevel inverters (MLIs) are one of the most promising classes of converters. As the name suggests, MLIs have a higher number of output voltage levels as compared to the two/three levels in traditional inverters. Due to higher output voltage levels, a main advantage of MLIs is the staircase-like output waveform, which resembles a sinusoid more closely than the traditional inverters. Therefore, MLIs offer a significantly lower THD [3]. Another advantage of MLIs pertinent to GCPS is that they can include multiple PV panels as an input. There are three main subclasses of multilevel inverters: (1) cascaded H-bridge (CHB), (2) diode clamped, and (3) flying capacitor [4]. The most common subclass is the CHB due to its modular structure, absence of energy storing elements, and the ability to isolate faults [5–8]. Practical multilevel inverters have typically five or more output voltage levels. Seven-level converters are most widely used as they offer a reasonable trade-off between performance and complexity. Therefore, in this paper, we have focused on seven-level inverters.

There are different variants of the CHB topology that are being employed in GCPS. The basic CHB topology [7, 8] provides excellent THD and MPP tracking due to the reason that each PV panel could be connected independently. However, it has a large number of semiconductor switches that

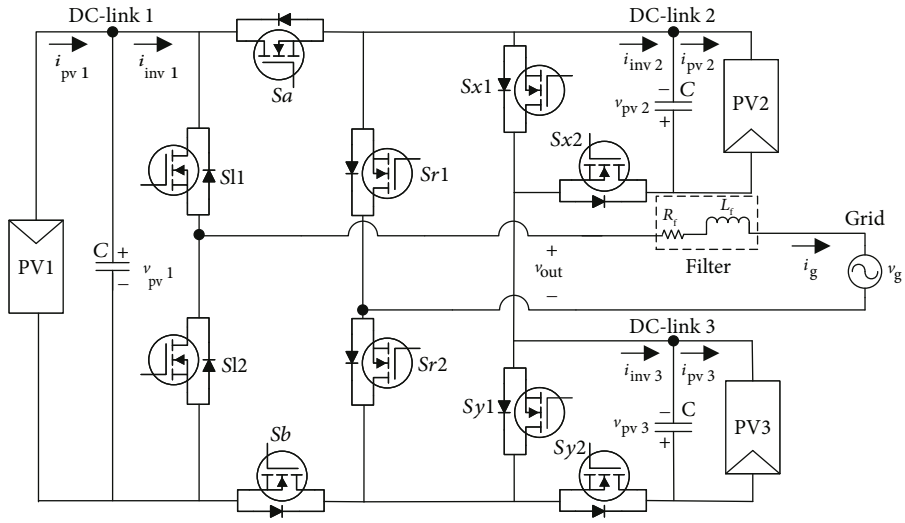

Figure 1: Proposed MLI-based grid-connected photovoltaic system.

increase the overall cost of the converter. The topology presented in [9] for a GCPS has decreased the number of switches as a trade-off to lower performance in terms of THD and MPPT tracking [10]. Another topology, called the novel H-bridge, was presented in [3, 11]. The novel H-bridge further reduced the number of switches. However, GCPS based on the topology in [9] and novel H-bridge has a drastically poor performance in MPP tracking when compared to GCPS based on the basic CHB topology. In this paper, we propose a new topology that is inspired from the novel H-bridge [3, 11] and an existing MLI structure in the literature [12]. The new topology has a lower number of switches than the basic CHB. Moreover, like basic CHB, the proposed topology also allows independent MPP tracking of each PV module, thereby giving a comparable performance to basic CHB in terms of MPP tracking.

As mentioned earlier, the employed control technique is the second key design component that affects the performance of a GCPS. Classical control schemes, such as PID, with a variety of modulation methods and compensations, have been used in CHB MLI-based GCPS [8]. A main drawback of classical control schemes is the large transient time and slow response [13]. Direct model predictive control (DMPC) is an emerging control scheme that is being used in power electronic converters. The distinguishing feature of DMPC is that the switches are controlled directly without a demodulator, as in PWM control. Advantages of DMPC include handling of plant nonlinearities, multiple control goals, explicit incorporation of constraints on inputs/states, and optimal control action. For most of the converters, DMPC has been shown to exhibit fast transient response, improved efficiency, and better overall control performance as compared to classical control schemes [14, 15].

In this paper, we have used DMPC for the control of the proposed topology and the GCPS. The key idea is to benefit from both the advantages of proposed MLI and DMPC to have an overall improved performance of the GCPS. To compare like with like, we collate our work with DMPC of GCPS based on three existing topologies mentioned earlier.

In Section 2, we propose a new multilevel inverter topology, describe its application in GCPS, and derive its mathematical model. In Section 3 of the paper, the proposed control scheme is explained in detail. The simulation results and comparison with existing work are given in Section 4 to show that the proposed MLI exhibits better performance than the three other recent converters. Finally, the conclusion is stated in Section 5.

2. Proposed Multilevel Inverter Topology

The circuit of the proposed MLI topology is shown in Figure 1. The converter has ten current bidirectional semiconductor switches labeled $Sl1$, $Sl2$, $Sr1$, $Sr2$, Sa, Sb, $Sx1$, $Sx2$, $Sy1$, and $Sy2$. The converter can have three input sources. For a GCPS, the sources are PV panels. Therefore, the input voltages are labeled v_{pv1}, v_{pv2}, and v_{pv3}. The part of the converter comprising of switches $Sx1$, $Sx2$, $Sy1$, and $Sy2$ is motivated from the structure presented in [12]. The remaining part of the converter is inspired from the novel H-bridge [3, 11].

The switch pair $(Sl1, Sl2)$ is complementary, that is, if one of the switches in the pair is off, and then, the other must be on. Similarly, the switch pairs $(Sr1, Sr2)$, (Sa, Sb), $(Sx1, Sx2)$, and $(Sy1, Sy2)$ are complementary. The four switches $Sl1$, $Sl2$, $Sr1$, and $Sr2$ constitute an H-bridge that allows inversion. The switches Sa and Sb allow selection of voltages on the right leg of the H-bridge, which enables multiple voltage levels at the output. The switches $(Sx1, Sx2)$ and $(Sy1, Sy2)$ allow inclusion/exclusion of sources v_{pv2} and v_{pv3}, respectively.

In the proposed topology, there are a total of 32 possible switching combinations. However, excluding the redundant combinations, only 15 combinations are used in operation. The 15 switching combinations and corresponding output voltages are shown in Table 1. In the table, 0 and 1 represent the off and on position of the switches, respectively. If the magnitude of all the voltage sources is kept equal, the proposed topology is able to generate seven-voltage levels. In

Table 1: Switching table for the proposed MLI topology.

Ind. j	Switching positions S (j)					v_{out}	v_{amp}
	$Sl1$, $Sl2$	$Sr1$, $Sr2$	Sa, Sb	$Sx1$, $Sx2$	$Sy1$, $Sy2$		
1	1, 0	0, 1	0, 1	0, 1	0, 1	v_{pv1}	
2	0, 1	1, 0	0, 1	0, 1	1, 0	v_{pv2}	$1v_{pv}$
3	0, 1	1, 0	0, 1	1, 0	0, 1	v_{pv3}	
4	1, 0	1, 0	0, 1	0, 1	1, 0	$(v_{pv1} + v_{pv2})$	
5	1, 0	1, 0	0, 1	1, 0	0, 1	$(v_{pv1} + v_{pv3})$	$2v_{pv}$
6	0, 1	1, 0	0, 1	0, 1	0, 1	$(v_{pv2} + v_{pv3})$	
7	1, 0	1, 0	0, 1	0, 1	0, 1	$(v_{pv1} + v_{pv2} + v_{pv3})$	$3v_{pv}$
8	0, 1	0, 1	0, 1	0, 1	0, 1	0	$0v_{pv}$
9	0, 1	1, 0	1, 0	0, 1	0, 1	$-v_{pv1}$	
10	1, 0	0, 1	1, 0	0, 1	1, 0	$-v_{pv2}$	$-1v_{pv}$
11	1, 0	0, 1	1, 0	1, 0	0, 1	$-v_{pv3}$	
12	0, 1	0, 1	1, 0	0, 1	1, 0	$-(v_{pv1} + v_{pv2})$	
13	0, 1	0, 1	1, 0	1, 0	0, 1	$-(v_{pv1} + v_{pv3})$	$-2v_{pv}$
14	1, 0	0, 1	1, 0	0, 1	0, 1	$-(v_{pv2} + v_{pv3})$	
15	0, 1	0, 1	1, 0	0, 1	0, 1	$-(v_{pv1} + v_{pv2} + v_{pv3})$	$-3v_{pv}$

the table, v_{out} is the output voltage of the inverter in terms of the voltage of each PV panel module. The voltage v_{amp} denotes the output voltage of the inverter for the case that the voltage of all PV panel modules is equal, that is, $v_{pv1} = v_{pv2} = v_{pv3} = v_{pv}$.

A main aspect of the proposed topology is that all the three input sources can be independently included/excluded in the output voltage. This feature is similar to the basic CHB topology, which is beneficial for independent MPP tracking of the PV panels.

Our main focus in this paper is on the use of the proposed topology in a grid-connected photovoltaic system (GCPS). The GCPS based on the proposed topology is shown in Figure 1. The GCPS consists of the proposed converter, PV panel modules, DC-link capacitors, low-pass filter, and the grid. A simple passive low-pass inductor filter L_f is used at the grid side to suppress the high-frequency harmonics. The resistance R_f is the equivalent series resistance of the inductor. For safety purposes, a transformer may be inserted at the grid side for isolation.

2.1. Modeling of the Proposed GCPS. The states in the proposed system are the DC-link capacitor voltages and grid/inductor current. The equation for the current can be found by applying Kirchhoff's voltage law (KVL) at the output port of the proposed system in Figure 1. The equation is as follows:

$$\frac{L\,\mathrm{di_g}}{\mathrm{dt}} = v_{out} - i_g * R_f - v_g, \tag{1}$$

where v_{out} is the output voltage of the MLI, v_g is the grid voltage, and i_g is the grid/inductor current. Discretization of the above equation by Euler's forward method yields the prediction equation for the grid current, which is

$$i_g^P = i_g(k+1) = i_g(k)\left(1 - \frac{R_f * T_s}{L}\right) + \frac{T_s}{L}\left(v_{out}(k) - v_g(k)\right), \tag{2}$$

where $i_g(k)$ and $i_g(k+1)$ are the values of grid current at time instant k and $k+1$, and T_s is the sampling time.

The equations for the DC-link voltages v_{pv1}, v_{pv2}, and v_{pv3} can be derived by applying Kirchhoff's current law (KCL) at the nodes of DC-links. The equations are given below:

$$\begin{aligned} \frac{C\,\mathrm{dv_{pv1}}}{\mathrm{dt}} &= i_{pv1}(k) - i_{inv1}(k), \\ \frac{C\,\mathrm{dv_{pv2}}}{\mathrm{dt}} &= i_{pv2}(k) - i_{inv2}(k), \\ \frac{C\,\mathrm{dv_{pv3}}}{\mathrm{dt}} &= i_{pv3}(k) - i_{inv3}(k). \end{aligned} \tag{3}$$

Discretization of the above equations yields

$$\begin{aligned} v_{pv1}^P &= v_{pv1}(k+1) = v_{pv1}(k) + \frac{T_s}{C}\left(i_{pv1}(k) - i_{inv1}(k)\right), \\ v_{pv2}^P &= v_{pv2}(k+1) = v_{pv2}(k) + \frac{T_s}{C}\left(i_{pv2}(k) - i_{inv2}(k)\right), \\ v_{pv3}^P &= v_{pv3}(k+1) = v_{pv3}(k) + \frac{T_s}{C}\left(i_{pv3}(k) - i_{inv3}(k)\right), \end{aligned} \tag{4}$$

where $v_{pv1}(k)$ is the DC-link 1 voltage, $v_{pv2}(k)$ is the DC-link 2 voltage, $v_{pv3}(k)$ is the DC-link 3 voltage, $i_{pv1}(k)$ is the

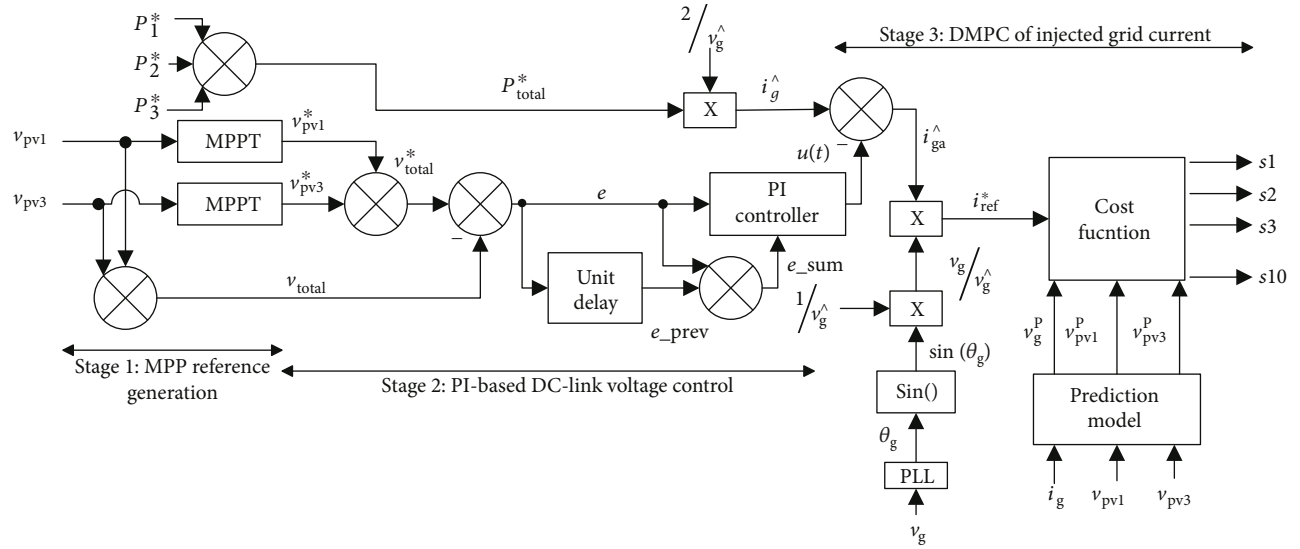

Figure 2: The basic controller diagram.

output current of PV1, $i_{pv2}(k)$ is the output current of PV2, $i_{pv3}(k)$ is the output current of PV3, C is the value of DC-link capacitors, and $i_{inv1}(k)$, $i_{inv2}(k)$, and $i_{inv3}(k)$ are the input currents of MLI.

3. Proposed Control Scheme

In this section, we describe the proposed control scheme for our GCPS. The control scheme is depicted in Figure 2. It consists of three main stages: (1) MPP reference generation, (2) PI-based DC-link voltage control, and (3) direct model predictive control of injected grid current. The initial two stages of the proposed scheme are standard in PV systems [7, 10]. However, the third stage of the control is based on the state-of-the-art direct model predictive control [14]. We will briefly describe the first two stages before a detailed explanation of the third stage.

The first stage generates the set point/reference to be used in stages 2 and 3. The first stage calculates the MPP reference values for the DC-link voltages v_{pv1}^*, v_{pv2}^*, and v_{pv3}^* and power P_1^*, P_2^*, and P_3^* for all the three PV panel modules. The reference values for MPP can change with the atmospheric conditions such as irradiance and temperature [16]. Therefore, the reference values need to be updated regularly.

The purpose of the second stage is to generate a reference grid current for the third stage. The reference grid current mainly depends on the total reference power calculated in stage 1 [7]. However, if the DC-link voltages are not at MPP, then the reference grid current has to be adjusted accordingly. The second stage uses a linear PI controller for this purpose that adjusts the reference peak value of the grid current $\hat{i}_g$ in accordance with the difference between reference and actual values of DC-link voltage. The peak value of the reference grid current is calculated as $\hat{i}_g = (P_{total}^*/\hat{v}_g) * 2$. The adjusted peak value of the reference grid current, denoted as $\hat{i}_{ga}$ in Figure 2, is calculated by adding $\hat{i}_g$ to the output of PI controller. Finally, the instantaneous reference i_{ref}^* of the grid current is calculated based on the adjusted peak reference $\hat{i}_{ga}$ and PLL.

The third stage is the DMPC of injected grid current which manipulates the semiconductor switches of the proposed multilevel inverter. The reference for the DMPC is i_{ref}^*. DMPC makes use of the discrete time model of the converter to calculate the optimal switching position among all the possible switching positions such that the reference tracking of grid current is ensured.

In DMPC, a cost function is minimized at each sampling instant k to select the optimal switching combination. We have used the following cost function

$$g = \left|i_{ref}^* - i_g(k+1)\right| + \lambda_v \left[\sum_{l=1}^{n} \left|v_{pv,l}^* - v_{pv,l}(k+1)\right|\right], \quad (5)$$

where i_{ref}^* is the reference for grid current, $i_g(k+1)$ is the actual grid current, $v_{pv,l}^*$ for $l = 1, 2, 3$ is the reference MPP voltage for each PV panel, $v_{pv,l}(k+1)$ for $l = 1, 2, 3$ is the actual voltage of each PV panel, n is the total number of input sources, and λ_v is the weighting factor. The cost function includes two terms. The first term penalizes the deviation of the actual current from the reference, which is the primary control objective of the third stage. The second term helps to regulate the DC-link voltages to their references. The weighting factor λ_v is used to specify the weightage of the second term in relevance to the first term.

Figure 3 depicts the flowchart of the DMPC algorithm. First of all, the controlled variables are measured, which are the grid current and DC-link voltages. The reference values of controlled variables are also taken from the first and second stages. It is also assumed that the best known cost g_{opt} is a very large number. The algorithm has to find the switching combination that gives the lowest cost among all the fifteen switching combinations that are listed in Table 1.

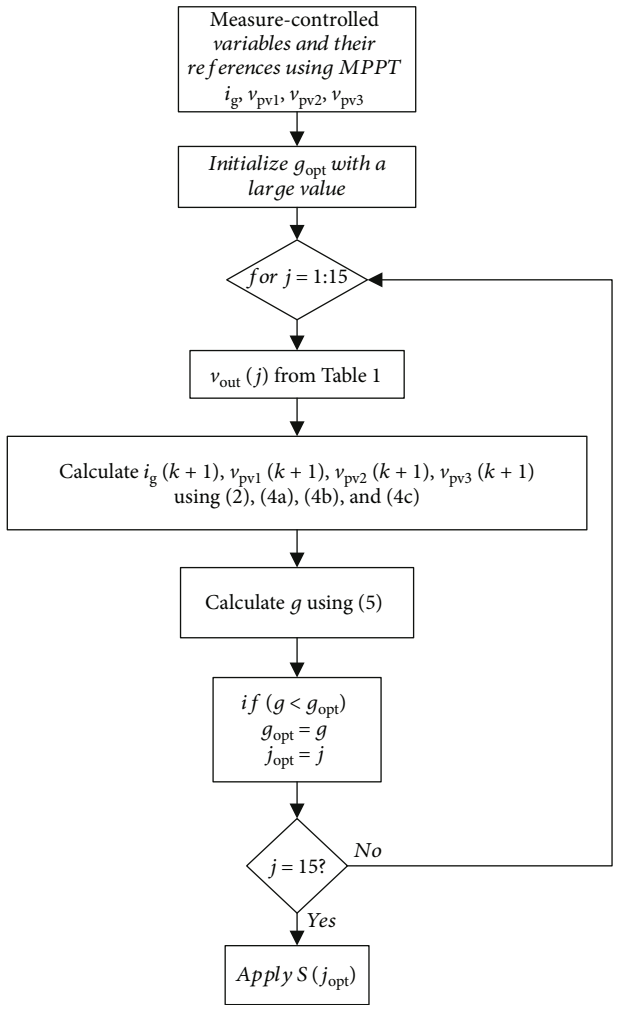

Figure 3: Flow diagram of the proposed control scheme.

For each switching combination, the output voltage of the MLI (v_{out}) is found by using Table 1. The grid current and DC-link voltages are predicted using the converter model (2) and (4). The cost (5) is calculated for the switching combination. If the cost is less than the optimal cost known so far, then the optimal cost g_{opt} and optimal switching sequence index j_{opt} are updated. At the end of the algorithm, the optimal switching combination is applied to the switches of the proposed multilevel inverter.

4. Simulation Results

A GCPS based on the proposed multilevel inverter and the proposed control scheme has been simulated in MATLAB Simulink. The PV panel module "Sharp ND-208U2" has been used as the source at all the three input ports of the converter. The rated maximum power of "Sharp ND-208U2" PV panel module is 208.05 Watts. The value of DC-link capacitors is kept at 15 mF. An inductor of 3 mH is used as filter. The ESR of the inductor is 0.2 Ω. Other parameters used in the simulation are specified in Table 2.

Table 2: System parameters.

Variable	Definition	Value
P_{total}	Nominal input power	624.1 W
$v^*_{pv1}, v^*_{pv2}, v^*_{pv3}$	Reference DC-link voltages	28.5 v
f	Frequency of grid	50 Hz
f_s	Switching/sampling frequency	20 kHz
L_f	Filtering inductor	3 mH
R_f	ESR	0.2 Ω
C	DC-link capacitor	15 mF
$\hat{v}_g$	Peak grid voltage	70 v

To evaluate the performance of the proposed converter, we have compared it with the simulation of three other converters. We have compared our proposed system to GCPS with DMPC based on (1) CHB [7], (2) topology in [9], and (3) novel H-bridge [11]. For each system, we obtained the simulation results for four different scenarios. In scenario 1, all the PV modules are working at 1000 W/m^2 irradiance and 25°C temperature. Scenario 1 is simulated for the first 0.4 seconds of the simulation. In scenario 2, which is from 0.4 s to 0.8 s of simulation time, solar irradiance of the module PV1 is changed from 1000 to 600 W/m^2, whereas in scenario 3, which is from 0.8 s to 1.2 s of simulation time, the solar irradiance of the module PV2 is changed from 1000 to 600 W/m^2. For the 4th scenario, the temperature of the module PV2 is changed from 25 to 35°C. Scenario 4 is from 1.2 s to 1.6 s of the simulation time.

The results of the comparison are given in Table 3. The comparison enlists the THD of grid current, THD of MLI output voltage, efficiency of the converter, and the number of semiconductor switches. Moreover, for each of the aforementioned four scenarios, the comparison table also shows the amount of power harvested from the panels.

The power extraction of the proposed converter is better than both the topology in [9] and the novel H-bridge. The power extraction is comparable to CHB. It is due to the reason that both the proposed converter and CHB can independently track the MPP of each PV panel module. In terms of efficiency, the proposed system fares much better than CHB and the topology in [9]. The efficiency of the proposed converter is comparable to novel H-bridge. The proposed converter offers the lowest THD in output voltage. The only performance criterion in which the proposed converter is outperformed by the others is the current THD. However, it is well within the acceptable limit of 5% in the standards [17]. Considering all the results in the table, the proposed converter arguably offers the best overall performance.

To provide a detailed analysis of the converter, Figure 4 illustrates the reference MPP DC-link voltage, actual DC-link voltages, reference MPP power, and the actual power extracted for each PV module. It can be seen that the proposed converter along with the proposed DMPC is able

Table 3: Comparison of systems.

GCPS Feature	DMPC and basic CHB-based GCPS [7]	DMPC and topology in [9] based on GCPS [10]	Novel H-bridge and DMPC-based GCPS	Proposed topology and DMPC-based GCPS
Grid current harmonics (%)	1.5–2	2.7–3.1	2.5–2.7	3.2
Output voltage harmonics (%)	28–30	29–36	24–32	22
Total power extracted during $0 < t < 0.4$ s (W)	623.50	613	618	623.25
Total power extracted during $0.4 < t < 0.8$ s (W)	543	542	542	542.7
Total power extracted during $0.8 < t < 1.2$ s (W)	462	385	395	462.65
Total power extracted during $1.2 < t \leq 1.6$ s (W)	456.9	383	391.5	456.95
Number of switches for 7-level MLI	12	9	6	10
η (%)	83	89	96	95

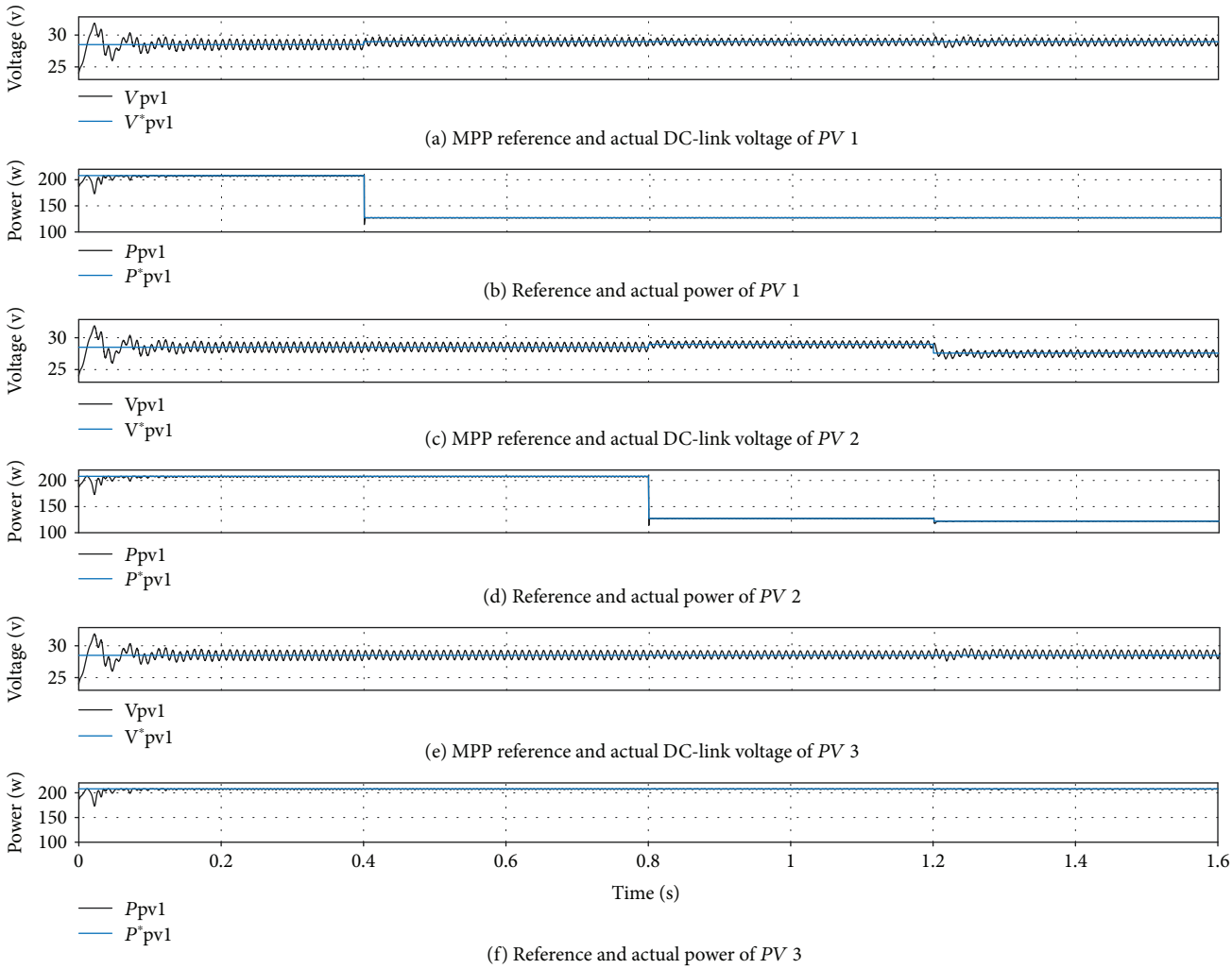

Figure 4: MPPT reference and actual DC-link voltage and power of the proposed MLI topology-based GCPS.

to track both the voltage and power references in all the four scenarios. For the purpose of comparison, we have shown the plots for novel H-bridge in Figure 5. The novel H-bridge has two input ports. In the figure, we see that the reference tracking of novel H-bridge-based GCPS maintains a constant error. Moreover, the effect of changes in atmospheric

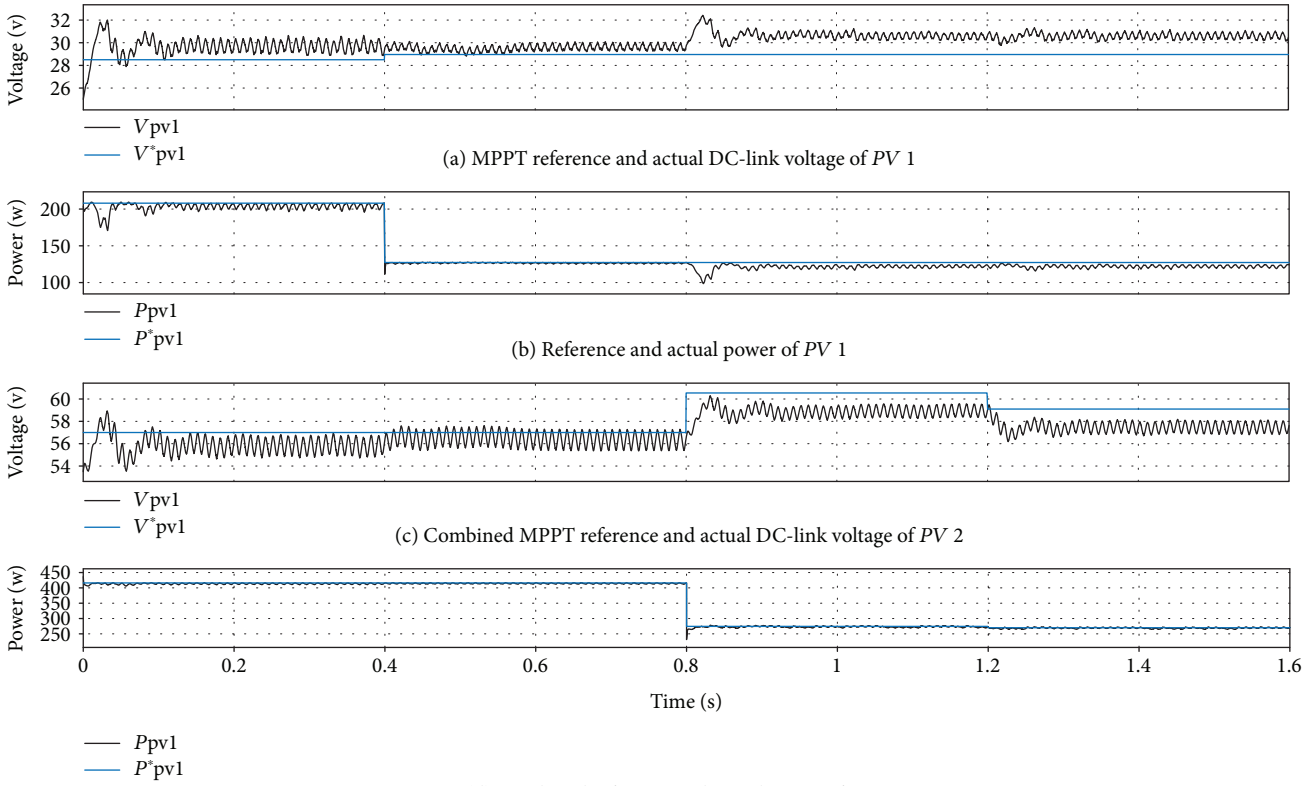

(a) MPPT reference and actual DC-link voltage of *PV* 1

(b) Reference and actual power of *PV* 1

(c) Combined MPPT reference and actual DC-link voltage of *PV* 2

(d) Combined reference and actual power of *PV* 2

Figure 5: MPPT reference and actual DC-link voltage and power of novel H-bridge-based GCPS.

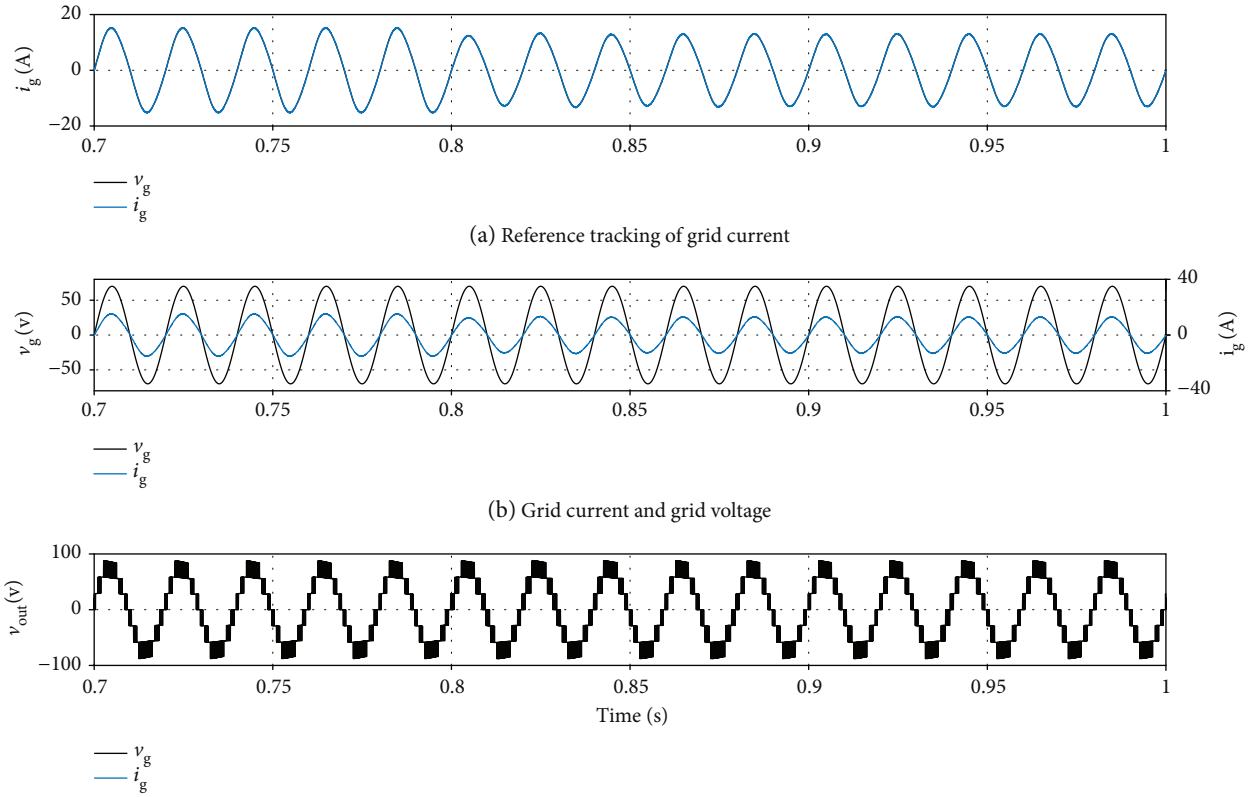

(a) Reference tracking of grid current

(b) Grid current and grid voltage

(c) Output voltage of multilevel inverter

Figure 6: Grid current, grid voltage, and output voltage of multilevel inverter.

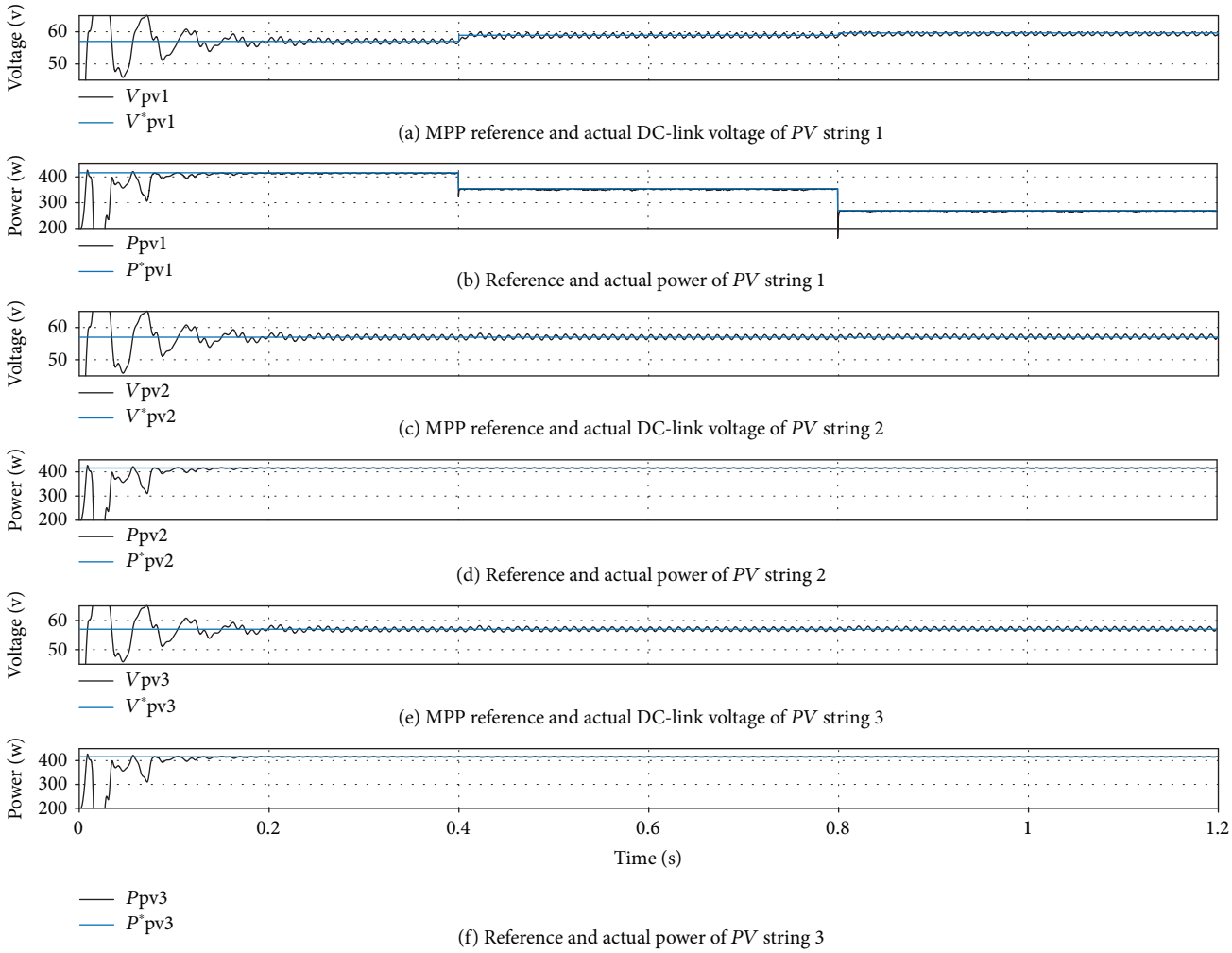

Figure 7: MPPT reference and actual DC-link voltage and power of the proposed MLI topology-based GCPS with PV strings as input sources.

condition of one PV module also influences the performance of other PV modules.

The reference grid current tracking of the proposed converter is shown in Figure 6(a). The figure is zoomed around 0.8 s. At $t = 0.8$ s, the reference grid current changes due to the change in reference power. However, the controller is able to quickly track the reference. The combined waveform of grid voltage and current is shown in Figure 6(b), which has no phase difference between them despite of changes in atmospheric conditions. The seven-level output voltage waveform of proposed MLI is shown in Figure 6(c).

4.1. Proposed System with PV Panels in String Formation. A common configuration of PV panels is the string formation [2]. In this section, we provide the simulation results of the proposed system with two series-connected PV modules (PV string) at each input port. The system is simulated for three different scenarios, and the results are shown in Figure 7. At the converter startup, all the PV strings, and their constituting PV panel modules, are operating at 1000 W/m^2 irradiance and 25°C temperature. The system achieves steady state in around 0.2 s. At $t = 0.4$ s, the irradiance of the first PV panel module of the PV string 1 is changed from 1000 W/m^2 to 800 W/m^2, whereas, at $t = 0.8$ s, the irradiance of the second PV panel module of PV string 1 is changed from 1000 W/m^2 to 600 W/m^2, while keeping the irradiance of first PV module at 800 W/m^2. As seen in Figure 7, at both of the above changes in irradiance, the proposed system is able to accurately track the MPP of PV string 1. Moreover, there is no impact on the MPP tracking of PV strings 2 and 3.

5. Conclusion

In this paper, we present a new multilevel inverter topology targeted for the application of grid-connected photovoltaic systems (GCPS). A GCPS based on the proposed converter and controlled via proposed DPMC is simulated. The proposed system is compared with GCPS with DMPC based on three other state-of-the-art topologies reported in the literature. The proposed converter is shown to be one of the best in terms of efficiency, power extraction, and voltage THD. The simulation results allow us to conclude that the

proposed topology offers the best overall performance in comparison to other topologies.

Data Availability

There is no underlying data in the research article.

Conflicts of Interest

The authors declare that there is no conflict of interest regarding the publication of this paper.

References

[1] S. B. Kjaer, J. K. Pedersen, and F. Blaabjerg, "A review of single-phase grid-connected inverters for photovoltaic modules," *IEEE Transactions on Industry Applications*, vol. 41, no. 5, pp. 1292–1306, 2005.

[2] S. Kouro, J. I. Leon, D. Vinnikov, and L. G. Franquelo, "Grid-connected photovoltaic systems: an overview of recent research and emerging PV converter technology," *IEEE Industrial Electronics Magazine*, vol. 9, no. 1, pp. 47–61, 2015.

[3] E. Babaei, S. Alilu, and S. Laali, "A new general topology for cascaded multilevel inverters with reduced number of components based on developed H-bridge," *IEEE Transactions on Industrial Electronics*, vol. 61, no. 8, pp. 3932–3939, 2014.

[4] J. Rodriguez, Jih-Sheng Lai, and Fang Zheng Peng, "Multilevel inverters: a survey of topologies, controls, and applications," *IEEE Transactions on Industrial Electronics*, vol. 49, no. 4, pp. 724–738, 2002.

[5] L. G. Franquelo, J. Rodriguez, J. Leon, S. Kouro, R. Portillo, and M. Prats, "The age of multilevel converters arrives," *IEEE Industrial Electronics Magazine*, vol. 2, no. 2, pp. 28–39, 2008.

[6] T. M., A. U. Khan, M. Luqman, M. B. Satti, M. Aaqib, and M. F. Khan, "Generation of isolated DC voltage sources for multilevel inverters," in *2015 Power Generation System and Renewable Energy Technologies (PGSRET)*, pp. 1–6, Islamabad, Pakistan, June 2015.

[7] P. Cortes, S. Kouro, F. Barrios, and J. Rodriguez, "Predictive control of a single-phase cascaded h-bridge photovoltaic energy conversion system," in *Proceedings of The 7th International Power Electronics and Motion Control Conference*, vol. 2, pp. 1423–1428, Harbin, China, June 2012.

[8] E. Villanueva, P. Correa, J. Rodriguez, and M. Pacas, "Control of a single-phase cascaded H-bridge multilevel inverter for grid-connected photovoltaic systems," *IEEE Transactions on Industrial Electronics*, vol. 56, no. 11, pp. 4399–4406, 2009.

[9] M. Mousa, M. E. Ahmed, and M. Orabi, "New converter circuitry for PV applications using multilevel converters," in *INTELEC 2009 - 31st International Telecommunications Energy Conference*, pp. 1–6, Incheon, South Korea, October 2009.

[10] M. Mosa, H. Abu-Rub, M. E. Ahmed, A. Kouzou, and J. Rodríguez, "Control of single phase grid connected multilevel inverter using model predictive control," in *4th International Conference on Power Engineering, Energy and Electrical Drives*, pp. 624–628, Istanbul, Turkey, May 2013.

[11] E. Babaei, S. Laali, and S. Alilu, "Cascaded multilevel inverter with series connection of novel H-bridge basic units," *IEEE Transactions on Industrial Electronics*, vol. 61, no. 12, pp. 6664–6671, 2014.

[12] E. Babaei and S. H. Hosseini, "New cascaded multilevel inverter topology with minimum number of switches," *Energy Conversion and Management*, vol. 50, no. 11, pp. 2761–2767, 2009.

[13] S. Vazquez, J. Rodriguez, M. Rivera, L. G. Franquelo, and M. Norambuena, "Model predictive control for power converters and drives: advances and trends," *IEEE Transactions on Industrial Electronics*, vol. 64, no. 2, pp. 935–947, 2017.

[14] J. Rodriguez, M. P. Kazmierkowski, J. R. Espinoza et al., "State of the art of finite control set model predictive control in power electronics," *IEEE Transactions on Industrial Informatics*, vol. 9, no. 2, pp. 1003–1016, 2013.

[15] R. P. Aguilera, Y. Yu, P. Acuna et al., "Predictive control algorithm to achieve power balance of cascaded H-bridge converters," in *2015 IEEE International Symposium on Predictive Control of Electrical Drives and Power Electronics (PRECEDE)*, pp. 49–54, Valparaiso, Chile, October 2015.

[16] D. P. Hohm and M. E. Ropp, "Comparative study of maximum power point tracking algorithms," *Progress in Photovoltaics: Research and Applications*, vol. 11, no. 1, pp. 47–62, 2003.

[17] M. Castilla, J. Miret, A. Camacho, J. Matas, and L. G. de Vicuna, "Reduction of current harmonic distortion in three-phase grid-connected photovoltaic inverters via resonant current control," *IEEE Transactions on Industrial Electronics*, vol. 60, no. 4, pp. 1464–1472, 2013.